

## Spatial Sensitivity and Calibration of 10HS Soil Moisture Sensors in Converted Paddy Fields for Practical Use

Chika ZUKEMURA\*, Teruhito MIYAMOTO and Hiroshi OSARI

Institute for Rural Engineering, National Agriculture and Food Research Organization, Tsukuba, Japan

### Abstract

This study confirmed a utility of a 10HS sensor, a capacitance sensor, in converted paddy fields to exploit the practical influence volume from our results and the corrected FSC function. Converted paddy fields in Japan are typically used to cultivate lowland rice or upland crops, and many of them have a problem of poor drainage when upland crops are cultivated. One of the major causes of poor drainage is a presence of a hardpan layer due to soil puddling for lowland rice cultivation. To monitor soil moisture above the hardpan layer without the influence of the hardpan layer, we identified the spatial sensitivity around the sensor and determined the applicability of the sensor with the factory-supplied calibration (FSC) function, including under near-saturated conditions. As a result, regarding the spatial sensitivity, the influence volume of the sensor from our result is much smaller than that reported by Cobos (2008), and we suggested that the sensors should be installed at least 1.5 cm above the boundary between the hardpan and plowed layers. Moreover, regarding the calibrations of the sensors, a corrected FSC function that can account for the bulk density was proposed.

**Discipline:** Agricultural Environment

**Additional key words:** bulk density, factory-supplied calibration function, hardpan layer, influence volume, near-saturated condition

### Introduction

Many rice farmers in Japan cultivate upland crops in paddy fields because annual rice consumption per person in Japan peaked in 1962 and has since decreased by approximately 50% (USDA 2021). The Ministry of Agriculture, Forestry and Fisheries of Japan subsidizes rice farmers if they cultivate upland crops in converted paddy fields. Therefore, paddy fields are typically used to cultivate either lowland rice or upland crops in Japan and are known commonly as “converted paddy fields.” Many converted paddy fields have a hardpan layer due to soil puddling during lowland rice cultivation. However, when upland crops are cultivated, rice farmers do not destroy the hardpan layer completely to avoid worsening the soil’s ability to hold water for cultivating rice. Therefore, the presence of the hardpan layer affects soil moisture movement in converted paddy fields. Specifically, water infiltrates vertically through the plowed soil layer and

arrives at the hardpan layer, and then, it continues to flow horizontally to the backfilled part of an underdrain (Tabuchi 2004) or slowly accumulates through the hardpan layer. During the cultivation of upland crops, converted paddy fields are susceptible to waterlogging with poor drainage. Thus, monitoring soil water dynamics above the hardpan layer is important for applying appropriate drainage management in converted paddy fields.

Electromagnetic methods, such as those using time-domain reflectometry (TDR) and capacitance sensors, are often applied in monitoring soil moisture. Several studies have used an EC-5 sensor (METER Group Inc., Pullman, WA, USA), a capacitance sensor, for laboratory experiments or field observations (e.g., Hamada et al. 2021, Mochizuki & Sakaguchi 2022, Sakaki et al. 2008). The merits of using this sensor are that it is relatively small and easy to handle. However, the 10HS sensor, which is a line of capacitance sensors

---

\*Corresponding author: [zukemura@affrc.go.jp](mailto:zukemura@affrc.go.jp)

Received 16 August 2022; accepted 23 March 2023.

manufactured by METER Group Inc., is more suitable for field observations because it has a larger influence volume than that of the EC-5 sensor. Therefore, the 10HS sensor was used in this study.

There are two concerns regarding measuring the volumetric water content,  $\theta$  [ $\text{m}^3 \text{m}^{-3}$ ], above the hardpan layer using 10HS sensors: spatial sensitivity around the sensor and the applicability of the sensor to measure near-saturated conditions. Spatial sensitivity around the sensor is related to the issue of how far away the sensor should be installed from the hardpan layer to avoid the influence of the layer. Numerous studies have confirmed the spatial sensitivity of TDR (e.g., Baker & Lascano 1989, Ferré et al. 1998, Nissen et al. 2003) and that of capacitance sensors (e.g., Schwartz et al. 2013, Vaz et al. 2013) experimentally and via numerical analysis. The sensitivity in the vicinity of the rod/prong is comparatively high, but it decreases rapidly at greater distances from the rod/prong. Moreover, Nissen et al. (2003) conducted an immersion experiment to measure the spatial sensitivity of TDR and found that the energy distribution around the TDR probe obtained by numerical analysis was similar to the distribution of the spatial sensitivity of TDR determined experimentally. However, Vaz et al. (2013) showed that the spatial sensitivity of a 5TE capacitance sensor suggested by the manufacturer was much greater than that actually measured during the immersion experiment. Although they also examined the 10HS sensor, they could not define its sensitivity via the immersion experiment because it can only measure apparent dielectric permittivity,  $\epsilon_a$ , up to 50, while the  $\epsilon_a$  value of water is approximately 80 (Decagon Devices 2016, METER Group 2019). To clearly define the spatial sensitivity around the 10HS sensor, it is necessary to adopt a different experimental approach instead of the immersion experiment.

The second concern is the accuracy of measured  $\theta$  values using the factory-supplied calibration (FSC) function, including near-saturated conditions, because  $\theta$  values above the hardpan layer often reflect near-saturated conditions. Several studies have already evaluated the performance of 10HS sensors with the FSC function (Domínguez-Niño et al. 2019, Ferrarezi et al. 2020, Vaz et al. 2013, Visconti et al. 2014). However, they mainly focused on the range of  $\theta$  values between field capacity and dry conditions in upland fields. Thus, this study conducted a calibration test to consider the applicability of the FSC function under near-saturated conditions in converted paddy fields.

The objectives of this study were to determine the spatial sensitivity around the 10HS sensor and to calibrate the sensor with the FSC function for in situ observation

in converted paddy fields. To this end, a new method was developed to examine the spatial sensitivity around the 10HS sensor. Moreover, calibrations of the sensor, including near-saturated conditions, were conducted. The applicability of the sensor was also evaluated by comparing the maximum  $\theta$  values obtained from in situ observations.

## Materials and methods

### 1. Outline of the 10HS sensors

10HS sensors use capacitance and frequency domain technology, and they consist of a black circuit board and two 10.2-cm prongs separated by an interval of 3.1 cm. Their oscillation is run at 70 MHz. The sensor output readings (“raw count values”) are transformed to  $\epsilon_a$  values by the FSC function (Eq. 1) provided by the manufacturer (METER Group 2019).

$$\begin{aligned} \epsilon_a = & 7.449 \times 10^{-11} \times (\text{raw count values})^4 \\ & - 1.969 \times 10^{-7} \times (\text{raw count values})^3 \\ & + 1.890 \times 10^{-4} \times (\text{raw count values})^2 \\ & - 6.691 \times 10^{-2} \times (\text{raw count values}) \\ & + 7.457. \end{aligned} \quad (\text{Eq. 1})$$

The manufacturer also provides the following FSC function (Eq. 2) that transforms raw count values to  $\theta$  values (METER Group 2019).

$$\begin{aligned} \theta = & 1.17 \times 10^{-9} \times (\text{raw count values})^3 \\ & - 3.95 \times 10^{-6} \times (\text{raw count values})^2 \\ & + 4.90 \times 10^{-3} \times (\text{raw count values}) \\ & - 1.92. \end{aligned} \quad (\text{Eq. 2})$$

The 10HS sensor’s user manual (Decagon Devices 2016, METER Group 2019) claims that the range of valid  $\epsilon_a$  measurements is between 1 and 50, and the range of valid  $\theta$  measurements is between 0.00 and  $0.57 \text{ m}^3 \text{m}^{-3}$  with each FSC function. Furthermore, the accuracy using the FSC function (Eq. 2) is reportedly  $\pm 0.03 \text{ m}^3 \text{m}^{-3}$  in mineral soils with solution electrical conductivity of  $<10 \text{ dS m}^{-1}$ , and the accuracy of the site-specific calibration function is reportedly  $\pm 0.02 \text{ m}^3 \text{m}^{-3}$  (METER Group 2019).

### 2. Spatial sensitivity around 10HS sensors

A drainage experiment was conducted to identify the spatial sensitivity of the 10HS sensors. An experimental container made of polyvinyl chloride with inner dimensions of  $20 \text{ cm} \times 35 \text{ cm} \times 35 \text{ cm}$  was prepared,

the 10HS sensor was suspended in the container as shown in Figure 1, and deionized water was supplied until the sensor was submerged. Next, deionized water was gradually drained until the raw count values started to be displayed on a ProCheck handheld reader (METER Group Inc.). Once the raw count values were displayed on the handheld reader, it started to record the raw count values and measure distances from the probe to the air/water interface using a ruler. It repeatedly recorded the values every time deionized water was drained at depths of 0.1 cm-0.5 cm until the raw count value was approximately 500.

We experimented with three 10HS sensors with six directions of the sensor in three repetitions per sensor. The measurement data were processed by the mean of these nine times per direction. In terms of the six directions, the details are as follows. The 10HS sensor placed horizontally with the probe in the vertical plane is referred to as “direction A” (Fig. 2(i)); similarly, the 10HS sensor placed horizontally with the probe in the horizontal plane is referred to as “direction B” (Fig. 2(ii)). Likewise, the 10HS sensor placed perpendicularly to the air/water interface is referred to as “direction C” (Fig. 2(iii)) or “direction D” (Fig. 2(iv)). Moreover, the characters “10HS” are printed on one side of the prong to distinguish between the sides. Specifically, in terms of direction A, the upper prong with the characters “10HS” is referred to as “direction A-1,” whereas the lower prong with the characters “10HS” is “direction A-2.” Similarly, in terms

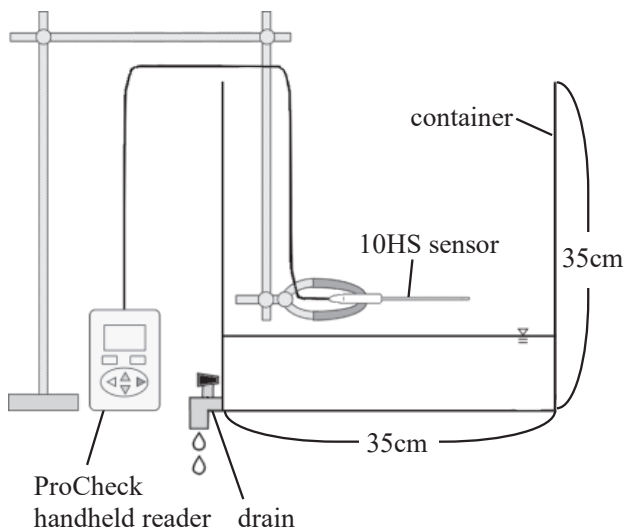


Fig. 1. Schematic of the setup for the drainage experiment

of direction B, the prong with the characters “10HS” facing upward is referred to as “direction B-1,” whereas that with the characters “10HS” facing downward is “direction B-2.”

The behavior of the sensor in layered systems is important for its calibration and performance evaluation. Moreover, it is necessary to confirm that the black circuit board of the 10HS sensor affects the sensor output. Concerning directions C and D, an additional analysis was performed. Bilayered systems that were described by Kargas & Soulis (2012) were applied to our results to examine the performance of the black circuit board. Comparisons were performed between the observed  $\epsilon_a$  values, which were calculated from the observed raw count values by the FSC function (Eq. 1), and the estimated  $\epsilon_a$  values, which were obtained as the refractive index averaging given by Eq. 3 and the arithmetic averaging given by Eq. 4 (Kargas & Soulis 2012).

$$\epsilon_{a-ref} = \frac{\sum_{i=1}^{N_L} L_i \sqrt{\epsilon_{a_i}}}{\sum_{i=1}^{N_L} L_i}, \quad (\text{Eq. 3})$$

$$\epsilon_{a-arith} = \frac{\sum_{i=1}^{N_L} L_i \epsilon_{a_i}}{\sum_{i=1}^{N_L} L_i}. \quad (\text{Eq. 4})$$

Here,  $\epsilon_{a-ref}$  is the apparent soil dielectric permittivity for the refractive index averaging,  $\epsilon_{a-arith}$  is the apparent soil

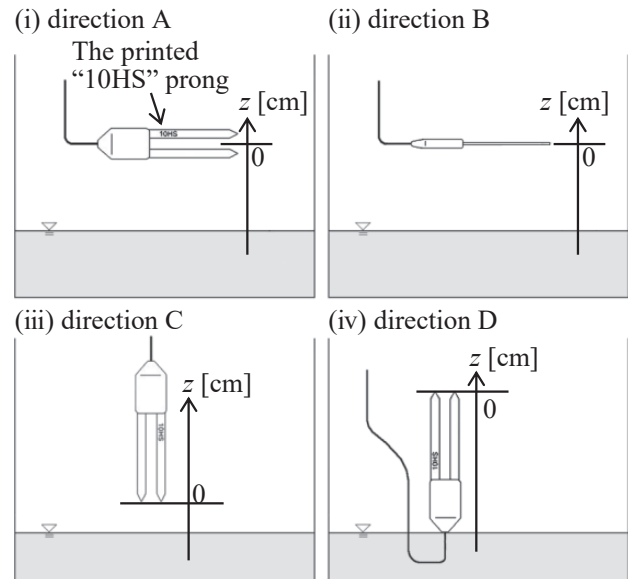


Fig. 2. Schematic of the experiment in different directions of 10HS sensors to identify its spatial sensitivity  
z describes the distance of the air/water interface from the center of the 10HS sensor or the tip of the prongs.

dielectric permittivity for the arithmetic averaging,  $L_i$  is  $i$ th layer thickness [cm],  $\epsilon_{ai}$  is the value of the apparent dielectric permittivity of the  $i$ th layer, and  $N_L$  is the number of layers.  $\sum_{i=1}^{N_L} L_i$  is the whole length of the bilayered system (Kargas & Soulis 2012).  $\epsilon_{a-ref}$  and  $\epsilon_{a-arith}$  were calculated under the following conditions: when the air/water interface position is 0.0 cm in direction C and -10.0 cm in direction D,  $\epsilon_{a-ref}$  values and  $\epsilon_{a-arith}$  values are 1, and when the air/water interface position is 10.0 cm in direction C and 0.0 cm in direction D,  $\epsilon_{a-ref}$  values and  $\epsilon_{a-arith}$  values are 50.

### 3. Calibration test of 10HS sensors for paddy soils

To consider the applicability of the FSC function (Eq. 2) under near-saturated conditions in converted paddy fields, a calibration test was conducted on eight paddy soil samples collected from converted paddy fields in Japan. The eight paddy soils are categorized as fluvisols or greysols, and their physicochemical properties are listed in Table 1. The contents of clay, silt, and sand were determined using the pipette method (Gee & Bauder 1986), and soil textures were classified following the International Society of Sciences guidelines (Murano et al. 2015). Humic acid content, which was used to evaluate the amount of organic matter, was determined using the method developed by the Ministry of Agriculture, Forestry and Fisheries of Japan based on the work of Kumada et al. (1967). The details are as follows: first, humic acid is extracted from soil samples with an alkali solution (0.1 M NaOH and 0.1 M  $\text{Na}_4\text{P}_2\text{O}_7$ ), and second, the absorbance is measured by colorimetric analysis at 530 nm. Two undisturbed samples (100 cm<sup>3</sup>) for each site were also taken to measure dry bulk density. Porosities were determined by calculations based on the absolute specific gravity of 2.6 Mg m<sup>-3</sup>.

The calibration test was conducted as follows. To begin with, soil samples were packed according to the method of Iwata et al. (2017). The soil sample was

packed into a polyvinyl chloride container (inner diameter of 20.2 cm and height of 20 cm) until a height of 12 cm (left side of Fig. 3) to follow each actual bulk density (Table 1), the prongs of the 10HS sensor were installed vertically by hand (center of Fig. 3), and the soil sample was repacked above a height of 6 cm to bury the entire sensor (right side of Fig. 3). Next, raw count values and the total weight of the container were recorded, and the gravimetric measurement of  $\theta$  values was performed. Then, the soil sample was taken out from the container and placed in a tray, mixed with added water, and left undisturbed overnight. These procedures were repeated until the soil samples were in near-saturated conditions. To obtain the site-specific calibration function, coefficients of a third-order polynomial equation were estimated using the least squares method for each soil sample using Microsoft Excel. Moreover, the root mean squared error (RMSE) values of the calibration functions were calculated using Eq. 5 to evaluate each calibration function.

$$RMSE = \sqrt{\frac{\sum_{i=1}^{N_s} (\theta_g - \theta_{10HS})^2}{N_s}} \quad (\text{Eq. 5})$$

Here,  $\theta_g$  is the volumetric water content obtained from gravimetric measurement,  $\theta_{10HS}$  is the volumetric water content calculated from Eq. 2, and  $N_s$  is the number of trials of the calibration test.

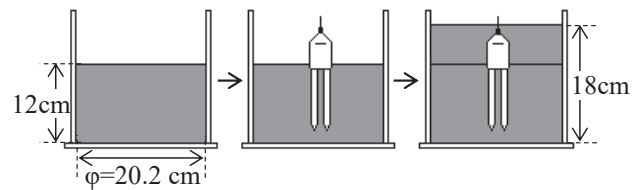


Fig. 3. Schematic illustrating the sensor installation steps of the calibration test

Table 1. Physicochemical properties of eight paddy soil samples

	Clay [%] 0.002 mm or less	Silt [%] 0.002-0.02 mm	Sand [%] 0.02-0.2 mm	Texture (ISSS method)	Humic acid [%]	Bulk density [Mg m <sup>-3</sup> ]	Porosity [m <sup>3</sup> m <sup>-3</sup> ]
(a) Mito	7.3	46.2	46.5	SiL	7.15	0.69	0.73
(b) Chikusei-1	21.9	27.7	50.4	CL	3.69	0.83	0.68
(c) Nagaoka	17.3	22.3	60.4	CL	1.65	0.87	0.67
(d) Omuta	22.2	29.4	48.4	CL	1.81	0.98	0.62
(e) Yasu	18.8	27.1	54.1	CL	1.42	1.11	0.57
(f) Chikusei-2	18.8	20.5	60.7	CL	2.40	1.13	0.57
(g) Munakata	31.8	30.6	37.5	LiC	1.51	1.17	0.55
(h) Anjo	30.6	20.0	49.4	LiC	1.40	1.30	0.50

To develop a simple correction method for the FSC function, the corrected FSC function accounting for bulk density was investigated using the observed values of the calibration test. Furthermore, we conducted in situ observation in eight converted paddy fields from which soil samples were collected for a calibration test to estimate the validity of the corrected FSC function under near-saturated conditions. The in situ observation was conducted in 2015 or 2016 during the period of soybean cultivation (from June-July to October-November). In these in situ observations, 10HS sensors were installed horizontally 2 cm-3 cm above the hardpan layer in direction B as described in Figure 2(ii), and raw count values were automatically recorded every hour using an Em5b logger (METER Group Inc.).

## Results

### 1. Spatial sensitivity around the 10HS sensor

Figure 4 shows the relationship between raw count values and the distance of the air/water interface from the center of the 10HS sensor in direction A. Negative distances indicate that the interface is located below the center of the 10HS sensor, as defined in Figure 2(i). When the interface was located at approximately 1.0 cm, “above range” was displayed on the handheld reader. In other words, the drainage experiments were conducted while the interface was located lower than 1.0 cm. To identify the range of large variations of raw count values, the average rate of change (ARC) was calculated by Eq. 6 from the observation data.

$$ARC = \frac{rcv_{i+1} - rcv_i}{h_{i+1} - h_i}. \quad (\text{Eq. 6})$$

Here,  $rcv_i$  is the raw count value when the air/water interface is located  $h_i$  (cm) above the center of the 10HS sensor, and  $i$  is the number of observed values. When the prong with the characters “10HS” was on the upper side (direction A-1), the raw count values decreased rapidly when the interface was located at 1.0 cm-0.0 cm. In addition, one peak of ARC appeared between the prongs (Fig. 4(i)). In contrast, when the prong with the characters “10HS” was on the lower side (direction A-2), the raw count values decreased in three steps. Hence, three peaks of ARC appeared (Fig. 4(ii)). Sakaki et al. (2008) described that one of the prongs of the EC-5 sensor was the “pulse-transmitted” prong and the other one was the ground prong, and they found a difference in sensitivity between these two prongs. Because the 10HS sensor is the successor of the EC-5 sensor, it probably

uses the same electrical processing. Therefore, according to Figure 4, the prong with the characters “10HS” is the pulse-transmitted prong with relatively significant sensitivity.

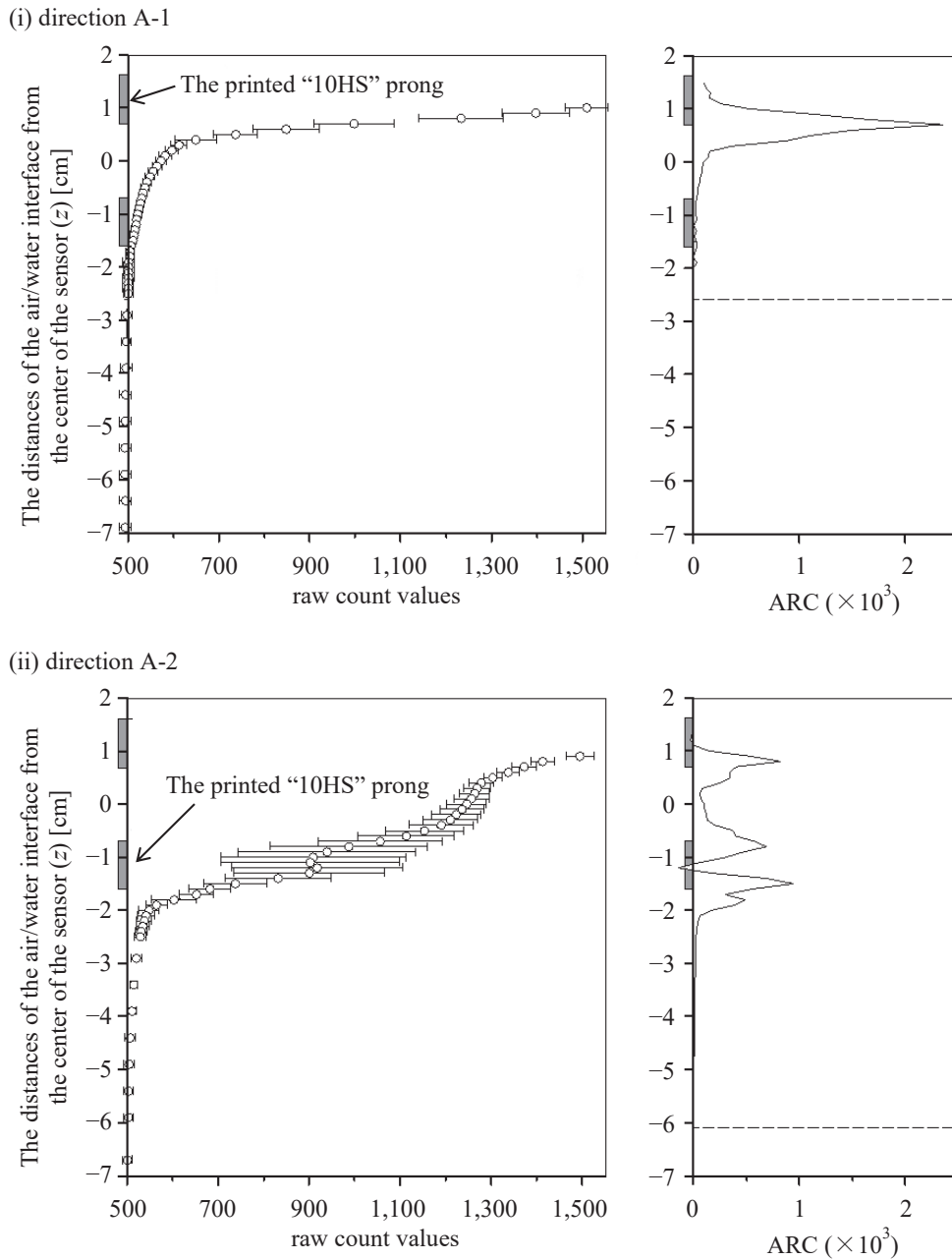
Figure 5 shows the relationship between raw count values and the distance of the air/water interface from the center of the 10HS sensor in direction B. Similar changes were observed regardless of whether the face of the prong with the characters “10HS” was above or below the surface. Measurements started when the air/water interface dropped to 0.3 cm. The raw count values decreased in two steps, and two peaks of ARC appeared on both sides. Spatial sensitivity included 1.5 cm below the center of the 10HS sensor.

Figure 6 shows the relationship between raw count values and the distance of the air/water interface from the tip of the prongs in directions C and D. When the sensor was installed downward, as defined in Figure 2(iii), positive distances indicated that the interface is located within the length of the prong. In contrast, when the sensor was installed upward, as defined in Figure 2(iv), negative distances indicated that the interface is located within the length of the prong. As the air/water interface got lower, the raw count values decreased for directions C and D. However, the raw count values obtained from direction C remained relatively high until the distance of the interface was approximately 4.0 cm (Fig. 6(i)). In contrast, the raw count values obtained from direction D decreased gradually and showed slightly higher values than those obtained from direction C even when most prongs were in the air (Fig. 6(ii)).

Figure 7 describes the relationship between the observed and estimated  $\varepsilon_a$  values. The observed  $\varepsilon_a$  values, which were calculated from the raw count value obtained in Figure 6, differed from each other because of the conditions surrounding the circuit board. The observed  $\varepsilon_a$  values obtained from position C followed the arithmetic averaging scheme at both lower and higher  $\varepsilon_a$  values and the refractive averaging scheme at intermediate  $\varepsilon_a$  values. In contrast, the observed  $\varepsilon_a$  values obtained from position D followed the refractive averaging scheme. These results suggest that installing the entire sensor into the soil provides more accurate soil dielectric properties.

### 2. Calibration test of 10HS sensors for paddy soils

The observed raw count values of the calibration test for the eight paddy soil samples were plotted as described in Figure 8. The site-specific calibration functions as described in Figure 8(a)-(h) were calculated from each third-order polynomial function shown in Table 2. For Mito and Chikusei-1, most of the measured data were plotted above the FSC function (Fig. 8(a), (b)), whereas



**Fig. 4. Relationship between raw count values and the distance of the air/water interface from the center of the sensor in direction A**

The prong with the characters "10HS" on the upper side is described as direction A-1, whereas the prong with the characters "10HS" on the lower side is described as direction A-2. Circles depict the measured plots, and the error bar on the graph depicts the standard deviation of the nine measurements. The gray square on the vertical axis depicts the setting direction of the prong of the 10HS sensor. The dashed line on the right side of the figure is the maximum possible measurement distance suggested by the manufacturer (Cobos 2008).

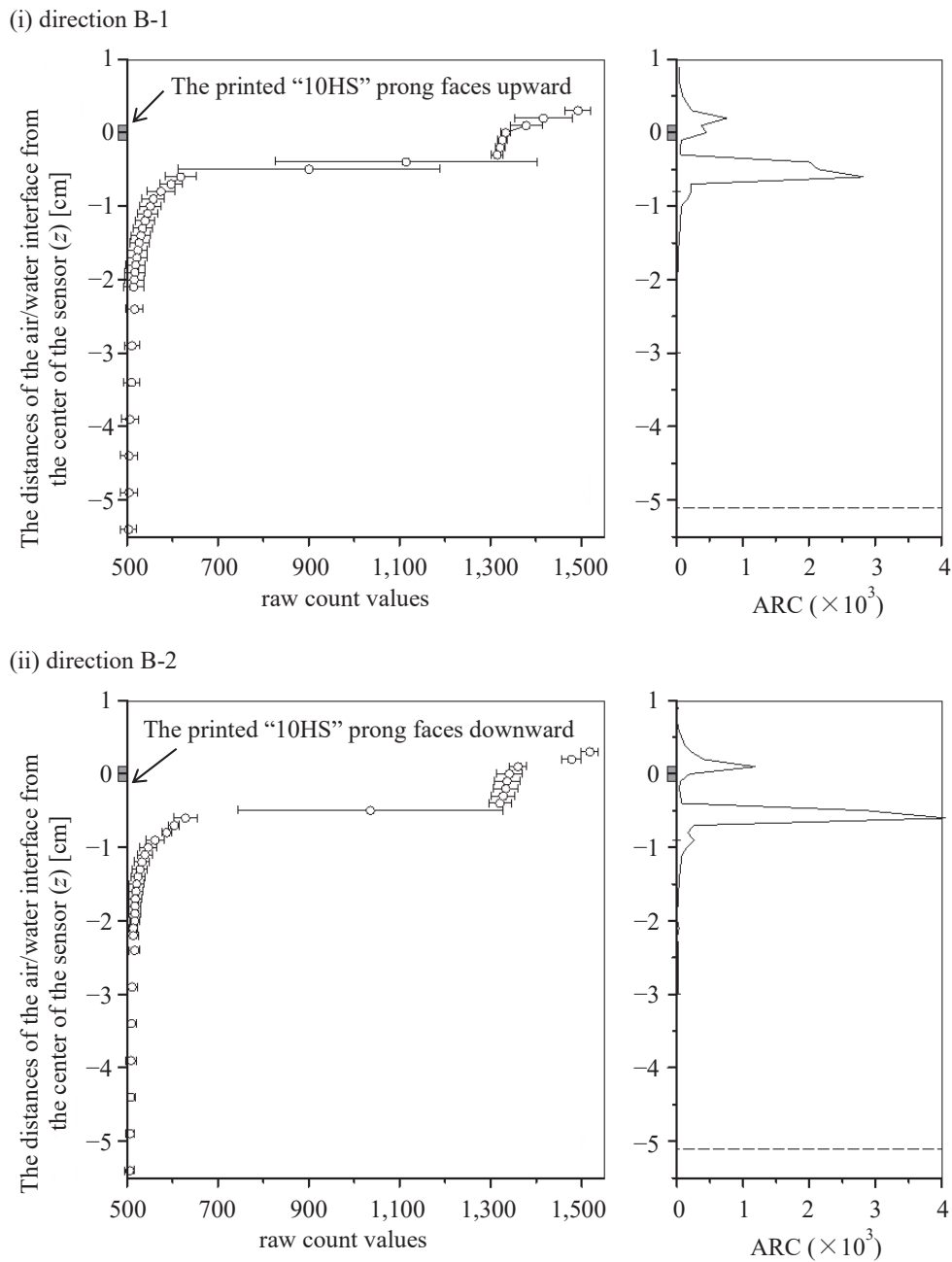


**Fig. 5. Relationship between raw count values and the distance of the air/water interface from the center of the sensor in direction B**

The prong with the characters “10HS” facing upward is described as direction B-1, whereas the prong with the characters “10HS” facing downward is described as direction B-2. Circles depict the measured plots, and the error bar on the graph depicts the standard deviation of the nine measurements. The gray square on the vertical axis depicts the setting direction of the prong of the 10HS sensor. The dashed line on the right side of the figure is the maximum possible measurement distance suggested by the manufacturer (Cobos 2008).

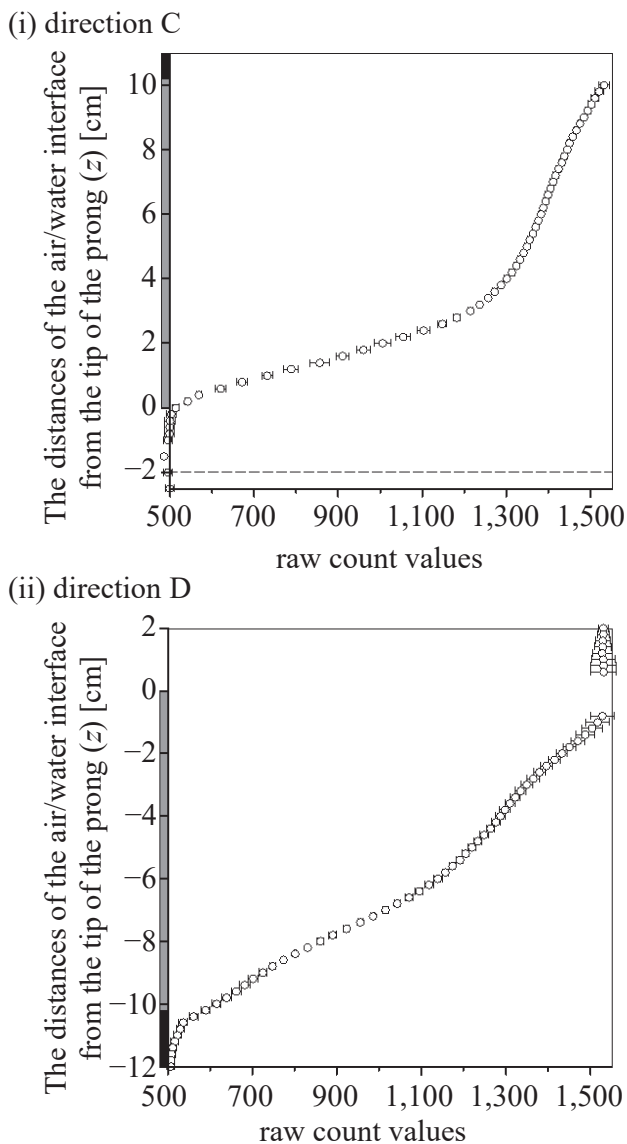


**Fig. 6. Relationship between the raw counts and the distance of the air/water interface from the tip of the prong in direction C or D**

Circles depict the measured plots, and the error bar on the graph depicts the standard deviation of the nine measurements. The gray square on the vertical axis depicts the setting direction of the 10HS sensor prongs, and the black square depicts the setting direction of the circuit board. The dashed line is the maximum possible measurement distance, according to Cobos (2008).

for Munakata and Anjo, most of the measured data were plotted below the FSC function (Fig. 8(g), (h)). In contrast to these soils, the FSC function fitted well for the measured data of Nagaoka, Omuta, Yasu, and Chikusei-2 (Fig. 8(c)-(f)). Table 3 describes the RMSEs of the FSC function and site-specific calibration functions. METER Group (2019) indicates that the accuracy of  $\theta$  values using the FSC function is  $\pm 0.03 \text{ m}^3 \text{ m}^{-3}$  in mineral soils. The

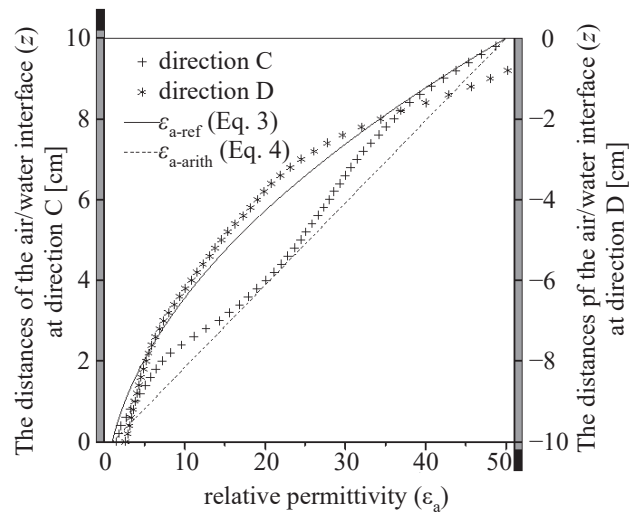


**Fig. 7. Relationship between the observed  $\epsilon_a$  values calculated from the result of Figure 6 in direction C or D and estimated  $\epsilon_a$  values according to the refractive averaging schemes and arithmetic one**  
Plus symbols depict the observed  $\epsilon_a$  values in direction C, and asterisks depict the observed  $\epsilon_a$  values in direction D. The gray squares on the vertical axis depict the setting direction of the 10HS sensor's prongs, and the black squares depict the circuit board's setting direction.

RMSEs of the FSC functions for the sites of Nagaoka, Omuta, Yasu, and Chikusei-2 were  $\leq 0.03 \text{ m}^3 \text{ m}^{-3}$  (Table 3). However, the measured data at Yasu around near-saturated conditions did not fit well for the FSC function (Fig. 8(e)).

## Discussion

### 1. Spatial sensitivity around the 10HS sensor

A drainage experiment was conducted to clearly define the spatial sensitivity around the 10HS sensor. The raw count values were observed to decrease rapidly upon moving the air/water interface away from the prongs, and they approached a constant value. During this stage of approaching a constant value, the environment surrounding the sensor was almost completely air, and the apparent dielectric permittivity was low. In other words, it was necessary to detect small differences to identify the spatial sensitivity around the 10HS sensor. To resolve this issue, we used the ARC to emphasize small differences in raw count values. Therefore, using the ARC and the drainage experiment, the spatial sensitivity of the 10HS sensors can be accurately determined.

Moreover, it is necessary to consider how far away the sensor should be installed from the hardpan layer to avoid the influence of the layers. The manufacturer showed the influence volume of 10HS sensors as an

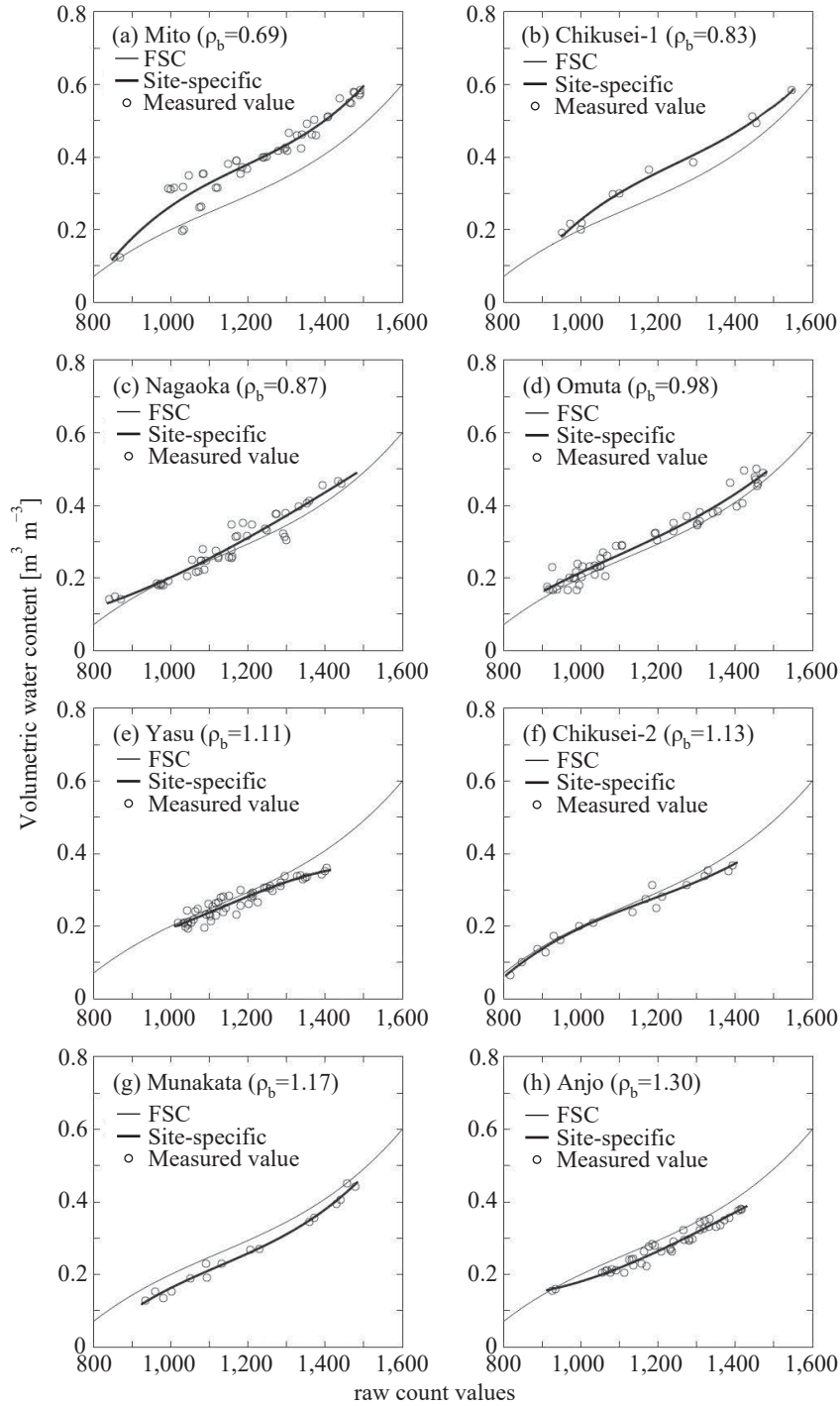


**Fig. 8. Relationship between raw count values and  $\theta$  values of the eight paddy soil samples**

Circles depict measured values, the thin lines depict the FSC function, and the thick lines depict the site-specific calibration function.

elliptical cylinder (Cobos 2008). Therefore, the influence volume from our results should be estimated for the elliptical cylinder with a base of approximately 4.1 cm at the maximum diameter and 3.0 cm at the minimum diameter (Fig. 9(iii)). This elliptical cylinder volume is much smaller than that reported by the manufacturer. In fact, the ARCs were zero at the distances suggested by the manufacturer (dashed line on the right of Figs. 4, 5). Therefore, the influence volume from our results must be made more available for practical use. Moreover, if 10HS sensors are installed in direction B-1 or direction B-2, they must be installed at least 1.5 cm above the boundary between the hardpan and plowed layers (Fig. 9(ii)).

**2. Calibration test of 10HS sensors for paddy soils**

Bulk density has a significant effect on capacitance sensors (Iwata et al. 2017, Mitsubishi & Mizoguchi 2014, Parvin & Degré 2016, Seyfried & Murdock 2001). To develop the corrected FSC function accounting for bulk densities, the intercept of the FSC function (Eq. 2) was corrected by adding a constant,  $\alpha$ , which is related to the bulk density (Eqs. 7, 8). Here,  $\alpha$  values were

$$\begin{aligned} \theta = & 1.17 \times 10^{-9} \times (\text{raw count values})^3 \\ & - 3.95 \times 10^{-6} \times (\text{raw count values})^2 \\ & + 4.90 \times 10^{-3} \times (\text{raw count values}) \\ & - 1.92 + \alpha, \end{aligned} \tag{Eq. 7}$$

**Table 2. Coefficients of the site-specific calibration function (third-order polynomial functions) to fit the measurements of each soil sample**

	$N_s$	$\theta = a \times (\text{raw count values})^3 + b \times (\text{raw count values})^2 + c \times (\text{raw count values}) + d$			
		$a$	$b$	$c$	$d$
(a) Mito	46	$2.1293 \times 10^{-10}$	$-7.5973 \times 10^{-6}$	0.0095	-3.8094
(b) Chikusei-1	11	$1.8404 \times 10^{-9}$	$-6.8951 \times 10^{-6}$	0.0091	-3.8427
(c) Nagaoka	45	$-1.6931 \times 10^{-10}$	$8.1006 \times 10^{-7}$	-0.0006	0.1820
(d) Omuta	51	$7.1011 \times 10^{-10}$	$-2.3117 \times 10^{-6}$	0.0030	-1.1764
(e) Chikusei-2	18	$1.1833 \times 10^{-9}$	$-4.1821 \times 10^{-6}$	0.0053	-2.1266
(f) Yasu	52	$-1.0068 \times 10^{-9}$	$3.4119 \times 10^{-6}$	-0.0034	1.1986
(g) Munakata	16	$1.5047 \times 10^{-9}$	$-5.0978 \times 10^{-6}$	0.0062	-2.4598
(h) Anjo	42	$-4.3418 \times 10^{-10}$	$1.8570 \times 10^{-6}$	-0.0021	0.8449

$N_s$  is the number of trials of the calibration test.

**Table 3. RMSEs of the FSC functions and the site-specific calibration functions**

	$\theta$ -RMSE (FSC)	$\theta$ -RMSE (Site-specific)
	[ $\text{m}^3 \text{m}^{-3}$ ]	[ $\text{m}^3 \text{m}^{-3}$ ]
(a) Mito	0.091	0.031
(b) Chikusei-1	0.048	0.014
(c) Nagaoka	0.030	0.025
(d) Omuta	0.029	0.022
(e) Yasu	0.026	0.016
(f) Chikusei-2	0.021	0.014
(g) Munakata	0.035	0.011
(h) Anjo	0.032	0.013

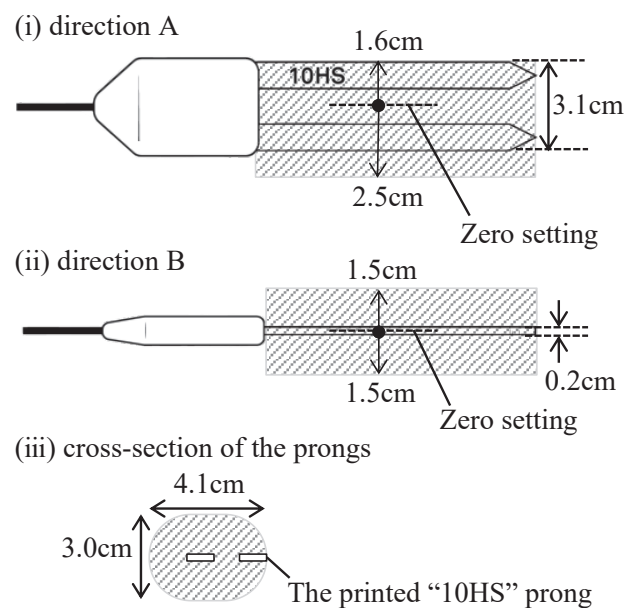


**Fig. 9. Influence volume of the 10HS sensor from our result (shaded area)**

$$\alpha = -0.18 \times (\text{bulk density}) + 0.19. \quad (\text{Eq. 8})$$

determined for eight soil samples to minimize the RMSEs by the least squares method (Fig. 10, Table 4).

The RMSEs of the corrected FSC function ( $0.017\text{-}0.038 \text{ m}^3 \text{ m}^{-3}$ ; Table 4) were close to the RMSE of the site-specific calibration function ( $0.011\text{-}0.031 \text{ m}^3 \text{ m}^{-3}$ ; Table 3). Therefore, the corrected FSC function is sufficiently accurate for monitoring  $\theta$  values in converted paddy fields that have different bulk densities.

Table 5 shows the maximum raw count values from in situ observations at the eight sites and the estimated  $\theta$  values by the FSC and corrected FSC functions. These results showed that the highest observed raw count value was 1,545, which was probably close to the upper limit of the measurements. Therefore, the 10HS sensor is applicable for monitoring  $\theta$  values for converted paddy soils, including under near-saturated conditions.

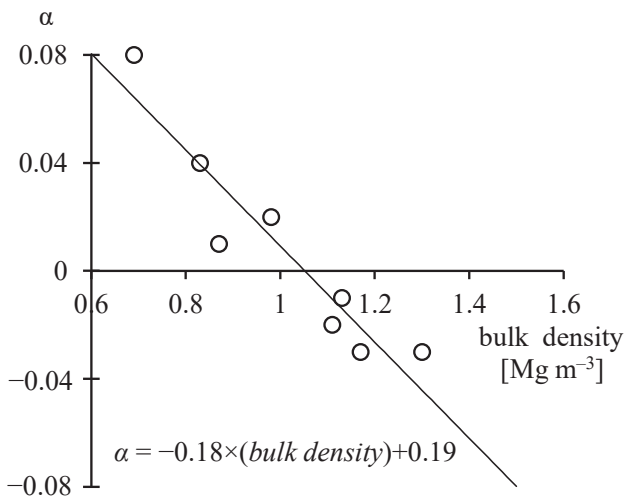


Fig. 10. Linear regression function between  $\alpha$  and bulk density

Table 4. Constant values,  $\alpha$ , and the RMSEs of the corrected FSC functions

	$\alpha$	$\theta$ -RMSE (corrected FSC) [ $\text{m}^3 \text{ m}^{-3}$ ]
(a) Mito	0.07	0.038
(b) Chikusei-1	0.04	0.023
(c) Nagaoka	0.03	0.031
(d) Omuta	0.01	0.024
(e) Yasu	-0.01	0.021
(f) Chikusei-2	-0.01	0.017
(g) Munakata	-0.02	0.018
(h) Anjo	-0.04	0.019

Moreover, to confirm the validity of the corrected FSC function under near-saturated conditions, the maximum  $\theta$  values between the FSC and corrected FSC functions were compared (Table 5). They were close to each other, except for at the site of Mito. However, the porosities were  $0.05\text{-}0.14 \text{ m}^3 \text{ m}^{-3}$  higher than the maximum  $\theta$  values from the corrected FSC function (Tables 1, 5). In several studies, it has been asserted that the entrapped air content is typically approximately  $0.10 \text{ m}^3 \text{ m}^{-3}$  for most soils (e.g., Fayer & Hillel 1986, Sakaguchi et al. 2005, Seymour 2000). Therefore, using the corrected FSC function to estimate  $\theta$  values in converted paddy fields is practical, including at the site of Mito.

## Conclusions

This study developed a new experimental method to identify the spatial sensitivity around the 10HS sensor. In a drainage experiment, it was revealed that by calculating the ARC, the spatial sensitivity of the 10HS sensor can be accurately determined. Moreover, the influence volume of the 10HS sensor was estimated for an elliptical cylinder with a base of approximately 4.1 cm at the maximum diameter and 3.0 cm at the minimum diameter. Thus, we suggest that 10HS sensors should be installed at least 1.5 cm above the boundary between the hardpan and plowed layers.

A simple correction method for the FSC function was developed for practical use in converted paddy fields. We suggested a corrected FSC function that can account for differences in bulk density (Eqs. 7, 8). The RMSEs of the corrected FSC function were close to the RMSEs of the site-specific calibration function. Moreover, considering the entrapped air content, the use of the corrected FSC function was reasonable, including under

Table 5. Maximum raw count values from *in situ* observation at the eight sites

	Maximum raw count values	Calculated from the maximum raw count values		
		$\varepsilon_a$ (Eq. 1)	$\theta$ (FSC) (Eq. 2)	$\theta$ (corrected FSC) (Eq. 7)
(a) Mito	1,545	53.5	0.54	0.61
(b) Chikusei-1	1,534	51.3	0.53	0.57
(c) Nagaoka	1,513	47.3	0.50	0.53
(d) Omuta	1,528	50.1	0.52	0.53
(e) Yasu	1,455	37.6	0.45	0.44
(f) Chikusei-2	1,469	39.7	0.46	0.45
(g) Munakata	1,504	45.6	0.50	0.48
(h) Anjo	1,500	44.9	0.49	0.45

near-saturated conditions. Therefore, it can be confirmed that 10HS sensors are practical for use in converted paddy fields to utilize the influence volume and the corrected FSC function.

## Acknowledgements

We gratefully acknowledge the assistance of Ms. K. Hirota, Ms. M. Inada, and Ms. M. Uesugi during the calibration test. This study was conducted as part of a research project conducted by the Ministry of Agriculture, Forestry and Fisheries of Japan, titled “Development of diagnostic methods and countermeasure techniques for overcoming high-yield inhibitory factors.”

## References

- Baker, J. M. & Lascano, R. J. (1989) The spatial sensitivity of time-domain reflectometry. *Soil Sci.*, **147**, 378-384. <http://dx.doi.org/10.1097/00010694-198905000-00009>.
- Cobos, D. (2008) Application Note “10HS volume of sensitivity.” Decagon Devices Inc., Pullman, WA. <https://www.ictinternational.com/content/uploads/2014/03/10HSVolume-of-Sensitivity.pdf>. Accessed on 1 June 2021.
- Decagon Devices Inc. (2016) 10HS Soil Moisture sensor manual. Decagon Devices Inc., Pullman, WA. <https://www.manualslib.com/manual/1256774/Decagon-Devices-10hs.html>. Accessed on 1 June 2021.
- Domínguez-Niño, J. M. et al. (2019) On the accuracy of factory-calibrated low-cost soil water content sensors. *Sensors*, **19**, 3101. <https://doi.org/10.3390/s19143101>.
- Fayer, M. J. & Hillel, D. (1986) Air encapsulation: I. Measurement in a field soil. *Soil Sci. Soc. Am. J.*, **50**, 568-572. <http://dx.doi.org/10.2136/sssaj1986.0361599500500030005x>.
- Ferrarezi, R. S. et al. (2020) Performance of soil moisture sensors in Florida sandy soils. *Water*, **12**, 358. <https://doi.org/10.3390/w12020358>.
- Ferré, P. A. et al. (1998) The sample areas of conventional and alternative time domain reflectometry probes. *Water Resour. Res.*, **34**, 2971-2979. <http://dx.doi.org/10.1029/98WR02093>.
- Gee, G. W. & Bauder, J. W. (1986) *Methods of soil analysis. Part I* (2<sup>nd</sup> ed.). Soil Science Society of America, American Society of Agronomy, Inc., Madison, WI.
- Hamada, K. et al. (2020) Evaluating maize drought and wet stress in a converted Japanese paddy field using a SWAP model. *Water*, **12**, 1363. <https://doi.org/10.3390/w12051363>.
- Iwata, Y. et al. (2017) Effect of sensor installation on the accurate measurement of soil water content. *Eur. J. Soil Sci.*, **68**, 817-828. <http://dx.doi.org/10.1111/ejss.12493>.
- Kargas, G. & Soulis, K. X. (2012) Performance analysis and calibration of a new low-cost capacitance soil moisture sensor. *J. Irrigat. Drain Eng.*, **138**, 632-641. [http://dx.doi.org/10.1061/\(ASCE\)IR.1943-4774.0000449](http://dx.doi.org/10.1061/(ASCE)IR.1943-4774.0000449).
- Kumada, K. et al. (1967) Humus composition of mountain soils in central Japan with special reference to the distribution of P type humic acid. *Soil Sci. Plant Nutr.*, **13**, 151-158.
- METER Group Inc. (2019) 10HS manual. METER Group, Inc. [https://publications.metergroup.com/Manuals/20426\\_10HS\\_Manual\\_Web.pdf](https://publications.metergroup.com/Manuals/20426_10HS_Manual_Web.pdf). Accessed on 1 June 2021.
- Mitsuishi, S. & Mizoguchi, M. (2014) Calibration of the capacitance type of ECH2O soil moisture sensors. *Dojyo no butsurisei (J. Jpn. Soc. Soil Phys.)*, **126**, 63-70. [https://doi.org/10.34467/jsoilphysics.130.0\\_19](https://doi.org/10.34467/jsoilphysics.130.0_19). [In Japanese with English abstract].
- Mochizuki, H. & Sakaguchi, I. (2020) Linear function for calibrating capacitance and frequency domain reflectometry (EC-5) for soil water monitoring by introducing slope-intercept relationship. *Soil Sci. Plant Nutr.*, **66**, 531-540. <http://dx.doi.org/10.1080/00380768.2020.1774319>.
- Murano, H. et al. (2015) Origin of the soil texture classification system used in Japan. *Soil Sci. Plant Nutr.*, **61**, 688-697. <http://dx.doi.org/10.1080/00380768.2014.998594>.
- Nissen, H. H. et al. (2003) Sample area of two- and three-rod time domain reflectometry probes. *Water Resour. Res.*, **39**, 1289. <https://doi.org/10.1029/2002WR001303>.
- Parvin, N. & Degré, A. (2016) Soil-specific calibration of capacitance sensors considering clay content and bulk density. *Soil Res.*, **54**, 111-119. <http://dx.doi.org/10.1071/SR15036>.
- Sakaguchi, A. et al. (2005) The effect of entrapped air on the quasi-saturated soil hydraulic conductivity and comparison with the unsaturated hydraulic conductivity. *Vadose Zone J.*, **4**, 139-144. <http://dx.doi.org/10.2136/vzj2005.0139>.
- Sakaki, T. et al. (2008) Empirical two-point  $\alpha$ -mixing model for calibrating the ECH<sub>2</sub>O EC-5 soil moisture sensor in sands. *Water Resour. Res.*, **44**, W00D08. <https://doi.org/10.1029/2008WR006870>.
- Schwartz, R. C. et al. (2013) Soil permittivity response to bulk electrical conductivity for selected soil water sensors. *Vadose Zone J.*, **12**. <https://doi.org/10.2136/vzj2012.0133>.
- Seyfried, M. S. & Murdock, M. D. (2001) Response of a new soil water sensor to variable soil, water content, and temperature. *Soil Sci. Soc. Am. J.*, **65**, 28-34. <http://dx.doi.org/10.2136/sssaj2001.65128x>.
- Seymour, R. M. (2000) Air entrapment and consolidation occurring with saturated hydraulic conductivity changes with intermittent wetting. *Irrig. Sci.*, **20**, 9-14. <http://dx.doi.org/10.1007/PL00006716>.
- Tabuchi, T. (2004) Improvement of paddy field drainage for mechanization. *Paddy Water Environ.*, **2**, 5-10. <http://dx.doi.org/10.1007/s10333-004-0034-7>.
- United States Department of Agriculture Foreign Agricultural Service (2021) Voluntary Report: MAFF increase crop diversification payments, Report No. JA2021-0032.
- Vaz, C. M. P. et al. (2013) Evaluation of standard calibration functions for eight electromagnetic soil moisture sensors. *Vadose Zone J.*, **12**. <https://doi.org/10.2136/vzj2012.0160>.
- Visconti, F. et al. (2014) Laboratory and field assessment of the capacitance sensors Decagon 10HS and 5TE for estimating the water content of irrigated soils. *Agric. Water Manag.*, **132**, 111-119. <http://dx.doi.org/10.1016/j.agwat.2013.10.005>.